Tidal and wind turbine simulation with the simulation code DOROTHY

C. Choma Bex, M.-A. Dufour, Y. Ben Belkacem, G. Pinon, G. Germain, E. Rivoalen

Tidal and wind turbine simulation with the simulation code DOROTHY

C. Choma Bex, M.-A. Dufour, Y. Ben Belkacem & G. Pinon
Laboratoire Ondes et Milieux Complexes - Normandie Univ, UNIHAVRE, CNRS, 76600 Le Havre.

G. Germain
IFREMER, Centre Manche Mer du Nord, 150 quai Gambetta, BP 699, 62321 Boulogne-sur-Mer.

E. Rivoalen
Laboratoire Ondes et Milieux Complexes - Normandie Univ, UNIHAVRE, CNRS, 76600 Le Havre,
Laboratoire de Mécanique de Normandie - Normandie Univ, INSA ROUEN, LMN, 76000 Rouen.

ABSTRACT: In the context of diversification toward renewable energies, wind and tidal turbines are set to play an important role. To this end, the simulation code DOROTHY uses the Vortex Particle Method, which offers a good compromise between physical realism and computational times. A possibility has recently been added for the account of ambient turbulence in the surrounding flow, using modules based on the *Synthetic Eddy Method* (SEM) and its divergence-free adaptation (DFSEM). Two representations are now available for the representation of the turbines: the historical option using boundary integral methods or a lifting line model. Thanks to all these developments, wakes and wake interactions of multiple turbines, with a possibility to account for ambient turbulence is now possible with DOROTHY. Furthermore, with the addition of the lifting line, performances evaluation and possible performance losses in realistic tidal or wind turbine farms conditions can now be treated.

1 INTRODUCTION

The simulation code DOROTHY has been under development for the past 15 years in collaboration between IFREMER (Institut Français de Recherche pour l'Exploitation de la Mer) and LOMC (Laboratoire Ondes et Milieux Complexes) of the Université Le Havre Normandie. A succession of theses and research projects have seen this numerical tool evolve with progressive additions of functionalities, in search of the methods best adapted to the representation of as many as possible realistic operating conditions present in tidal or wind turbine farm sites.

A current stake is the evaluation of the fluctuating loads encountered by the turbine blades because these loads dimension blades lifetime from a material fatigue point of view. To tackle this issue with a simulation code, ambient turbulence have to be accounted for and the framework has to allow turbine interactions.

This paper will showcase the alternatives currently implemented in this simulation code for the representation of the turbines, the account for ambient turbulent intensity in the Lagrangian framework considered, and the possibilities for the simulation of turbine interactions under farm conditions.

2 ELEMENTS OF IMPLEMENTATION IN DOROTHY

2.1 *The Vortex Particle Method*

The simulation code DOROTHY uses the Vortex Particle Method (Rehbach 1977, Lewis 1991, Cottet & Koumoutsakos 2000, Pinon et al. 2012). This Lagrangian method is based on a discretisation of the fluid into vorticity carrying particles. The governing equations for this unsteady model are the Navier-Stokes equations in their velocity-vorticity $(\boldsymbol{u}, \boldsymbol{\omega})$ formulation:

$$\nabla \cdot \boldsymbol{u} = 0, \tag{1}$$

$$\frac{D\boldsymbol{\omega}}{Dt} = (\boldsymbol{\omega} \cdot \nabla)\boldsymbol{u} + \nu \Delta \boldsymbol{\omega}, \tag{2}$$

where $\boldsymbol{u}$ is the velocity field, $\boldsymbol{\omega} = \nabla \times \boldsymbol{u}$ the vorticity field, and ν the cinematic viscosity.

The fluid domain is discretised into N_p particules, each particle i represented by its position $\boldsymbol{X}_i$ and its vortical weight $\boldsymbol{\Omega}_i$ and assigned a volume V_i. The transport of these particles is characterised by the equation:

$$\frac{\mathrm{d}\boldsymbol{X}_i}{\mathrm{d}t} = \boldsymbol{u}(\boldsymbol{X}_i) = \boldsymbol{U}_i \ , \tag{3}$$

which is then integrated using time stepping schemes.

This brings us to a discrete version of Equation (2), dictating the evolution of the vorticity transported by each particle i:

$$\frac{\mathrm{d}\boldsymbol{\Omega}_i}{\mathrm{d}t} = \underbrace{(\boldsymbol{\Omega}_i \cdot \nabla)\,\boldsymbol{U}_i}_{\text{stretching term:}\boldsymbol{\mathcal{S}}_i V_i} + \underbrace{\nu[\Delta\boldsymbol{\omega}]_{\boldsymbol{x}=\boldsymbol{X}_i} V_i}_{\text{diffusion term:}\boldsymbol{\mathcal{L}}_i V_i}. \tag{4}$$

In order to solve this equation, the vortex particle method uses a Helmholtz decomposition of the velocity field:

$$\boldsymbol{U} = \underbrace{\nabla \times \boldsymbol{\psi}}_{\boldsymbol{U}^\psi} + \underbrace{\nabla\phi}_{\boldsymbol{U}^\phi} + \boldsymbol{U}^\infty; \tag{5}$$

where the velocity components can be summarized as follows:

- $\boldsymbol{U}^\psi$ is a rotational component representing the interaction between fluid particles, the heart of the Vortex Particle Method.
- $\boldsymbol{U}^\phi$ is a potentiel component representing the influence of the solid bodies (i.e. the tidal or wind turbines).
- $\boldsymbol{U}^\infty$ represents the upstream incoming velocity, usually treated as a constant value, which can however be adapted to include an account for ambient turbulence as will be seen further throughout this work.

The rotational component $\boldsymbol{U}^\psi$ representing the influence of the fluid particles can be expressed in its discretized form:

$$\boldsymbol{U}^\psi(\boldsymbol{x}) = \sum_{i=1}^{N_p} \boldsymbol{K}_\epsilon(\boldsymbol{x}, \boldsymbol{X}_i) \times \boldsymbol{\Omega}_i \,, \tag{6}$$

with $\boldsymbol{K}_\epsilon$ a regularisation of the Biot and Savart kernel $\boldsymbol{K}$. This direct computation carried out for each single particle making up the fluid domain is accelerated using a *treecode* type algorithm based on the works of (Lindsay & Krasny 2001).

For more in depth descriptions of the functioning of these methods and of their implementation, see (Pinon et al. 2017, Mycek 2013). Possible treatments of the diffusion term are explored in (Mycek et al. 2016). Interaction of the diffusion term with the ambient turbulence model is described further on in (Choma Bex et al. 2020).

2.2 *Towards multiple possibilities for the simulation of a turbine*

2.2.1 *Simulation of a turbine by integral method and turbine interactions*

The component $\boldsymbol{U}^\phi$ appearing in the Helmholtz decomposition of Equation (5) can represent the influence of the turbine bodies by different methods. The first possibility used in the Dorothy simulation code since its beginnings is based on a singularity method using a dipole distribution on a zero-thickness surface mesh.

Derived from a continuous solution to the Poisson Equation $\boldsymbol{\nabla}^2\,\phi = 0$, this component can then be formulated as:

$$\boldsymbol{u}^\phi(\boldsymbol{x}) = \sum_{j=1}^{N_f} \left(\mu_j \int_{\boldsymbol{y}\in\mathscr{S}_j} \boldsymbol{\nabla}_{\boldsymbol{x}} \left[\boldsymbol{K}(\boldsymbol{x},\boldsymbol{y}) \cdot \boldsymbol{n}_j\right] dy \right) \,, \tag{7}$$

assuming its application to a surface $\mathscr{S}$ discretized into individual faces $\left(\mathscr{S} = \cup_{j=1}^{N_f} \mathscr{S}_j\right)$ of normals $\boldsymbol{n}_j$ and constant dipole distribution intensities μ_j.

Using a series of geometrical manipulations, this integral formulation is transformed into:

$$\boldsymbol{U}^\phi(\boldsymbol{x}) = \frac{1}{4\pi} \sum_{j=1}^{N_f} \left(\mu_j \sum_{k=1}^{4} \boldsymbol{\alpha}_j^k(\boldsymbol{x}) \right) \,. \tag{8}$$

The justification of this simplification and the detailed formulation of the coefficient $\boldsymbol{\alpha}_j^k$ based on the geometry of each mesh face $\mathscr{S}_j$ can be found in multiple references, such as (Bousquet 1990, Mycek 2013).

The dipole distribution $(\mu_j)_{j=1}^N$ must be calibrated so as to ensure the complete velocity of the fluid verifies the slip condition on the mesh surface $\mathscr{S}$:

$$\left(\boldsymbol{U}^\phi + \boldsymbol{U}^\psi + \boldsymbol{U}^\infty\right) \cdot \boldsymbol{n} = \boldsymbol{U}_{\mathscr{S}} \cdot \boldsymbol{n} \,, \tag{9}$$

where for the case of a classic wind or tidal turbine the relative velocity $\boldsymbol{U}_{\mathscr{S}}$ is the velocity induced by the rotation of the turbine.

By replacing the potential component $\boldsymbol{U}^\phi$ by its formulation of Equation (8) in the slip condition of Equation (9), a linear system of size $N_f \times N_f$ and unknown $\boldsymbol{\mu} = (\mu_j)_{j=1}^N$ can be obtained:

$$\overline{\overline{\boldsymbol{A}}}\boldsymbol{\mu} = \boldsymbol{b} \,. \tag{10}$$

The coefficients A_{ij} of the influence matrix $\overline{\overline{\boldsymbol{A}}}$ are given by:

$$A_{ij} = \frac{1}{4\pi} \sum_{k=1}^{4} \boldsymbol{\alpha}_j^k(\boldsymbol{X}_i) \cdot \boldsymbol{n}_i \,, \tag{11}$$

and the coefficients b_i of the right-hand-side vector $\boldsymbol{b}$:

$$b_i = \left[\boldsymbol{U}_{\mathscr{S}}(\boldsymbol{x}_i) - \boldsymbol{U}^\psi(\boldsymbol{x}_i) - \boldsymbol{U}^\infty\right] \cdot \boldsymbol{n}_i \,. \tag{12}$$

This resolution completes the numerical computation of the potential velocity $\boldsymbol{U}^\phi$ using a dipole distribution on a zero-thickness mesh.

However the numerical treatment of the resolution of the linear system can remain an important challenge, all the more so in the case of multiple interacting turbines requiring an update of the influence matrix at each time step (see Figure 1). For such further advanced configurations which can be more demanding in terms of computational times, an iterative Bi-CGSTAB type solver was chosen. The details of its implementation and the ensuing results can be found in (Mycek et al. 2017).

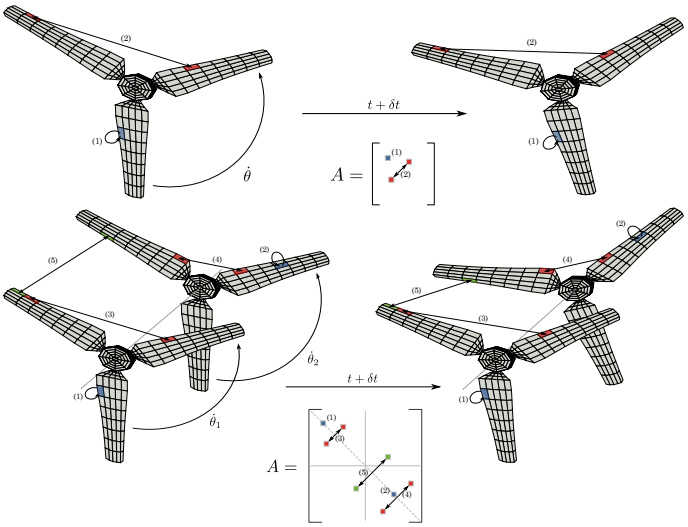

Figure 1: Schematic representation of the consequences on the matrix $\overline{\overline{\boldsymbol{A}}}$ of the passage from a single to a multi-turbine interaction configuration.

Even though this method has been used for years in the simulation code Dorothy and produces satisfying results in terms of wakes, such has not been the case in terms of performance results (Pinon et al. 2012). Thus some alternatives have recently been explored, among which a first more complex possibility aims to allow the computation of efforts on a fully rendered three-dimesional detailed geometry, and a second more efficient possibility gives access to immediate performance results using a lifting line representation.

2.2.2 *Towards a simulation of the turbine by an integral method for a solid body*

In order to improve the current results in terms of efforts on the machines as well as their detailed and more realistic geometry, some developments have been undertaken on the implementation of an alternative formulation for the representation of the turbine bodies. This passage from a zero-thickness mesh

Figure 2: Passage of the representation of the tidal or wind turbine blades reduced to their mean camber zero-thickness surface to a fully rendered three-dimensional thick representation.

to a fully three-dimensional surface mesh (see Figure 2) begins with a revision of the dipole singularity method described in the previous paragraph to include additional source type singularities. Such a combination of dipole and sources singularities is recurring throughout the literature (Riziotis & Voutsinas 2008, Greco et al. 2004, Salvatore et al. 2015, Salvatore et al. 2003). The implementation considered here is based on a decomposition taken from (Morino 1990). Some details of the justification and derivation of this decomposition can be found in the thesis (Choma Bex 2021).

Beginning once again with the Helmholtz decomposition of the velocity, a series of mathematical and geometrical manipulations can lead to the formulation of the velocity field:

$$\boldsymbol{u}(\boldsymbol{x}) = \underbrace{-\int_{\boldsymbol{y}\in\mathscr{V}} \boldsymbol{K}(\boldsymbol{x},\boldsymbol{y}) \times \boldsymbol{\omega}(\boldsymbol{y}) dy}_{①} + \underbrace{\boldsymbol{\nabla}_{\boldsymbol{x}} \left[\int_{\boldsymbol{y}\in\mathscr{S}} G(\boldsymbol{x},\boldsymbol{y}) \sigma(\boldsymbol{y}) dy \right]}_{②}$$
$$\underbrace{- \boldsymbol{\nabla}_{\boldsymbol{x}} \left[\int_{\boldsymbol{y}\in\mathscr{S}} \boldsymbol{K}(\boldsymbol{x},\boldsymbol{y}) \cdot (\mu(\boldsymbol{y})\boldsymbol{n}(\boldsymbol{y})) dy \right]}_{③} + \boldsymbol{u}_\infty \tag{13}$$

where we can recognize in the terms ① and ③ the components representing the influence of fluid particles and of a distribution of surface dipoles μ covered previously, to which is added a new term ② corresponding to the influence of a source intensity distribution of known intensities $\sigma = \boldsymbol{n} \cdot \boldsymbol{u}_{\mathscr{S}}$.

The combination of these elements is sufficient for the simulation of fully-rendered thick turbines along with their wake. The next step is the addition of a computation of the efforts on each face of the new meshes. To this end, we use the method from (Ogami 2017), which incorporates a calculation of the velocity potential on mesh faces to which is then applied the Bernoulli relation.

Using the simple relation between potential and velocity along a segment $\varphi_{AB} = \int_A^B \boldsymbol{u} \cdot \boldsymbol{dr}$, a rectangular matrix can be constructed to translate this relation applied to the centers of pairs of neighboring mesh faces:

$$\varphi_{j+1} - \varphi_j \simeq \boldsymbol{u}_j \cdot \boldsymbol{dr}_j + \boldsymbol{u}_{j+1} \cdot \boldsymbol{dr}_{j+1} \ , \tag{14}$$

the resolution of which gives access to a value of the velocity potential on each face j of the mesh.

We can then use Bernoulli's relation, a practice widely used in potential codes for good quality performance results outside of the regions of stall (Salvatore et al. 2015, Salvatore et al. 2018):

$$p_j = -\rho \left(\frac{\partial \varphi_j}{\partial t} + \frac{1}{2} |\boldsymbol{u_j}|^2 \right) \ , \tag{15}$$

with $\boldsymbol{u_j}$ the complete velocity known at the center the mesh face j. The pressure force can thus be deduced:

$$\boldsymbol{F} = -\sum_{j=1}^{N_f} p_j \boldsymbol{n_j} \Delta_{S_j} \ , \tag{16}$$

with Δ_{S_j} the area of the mesh face j.

The preliminary validations of these computations are also exposed in the thesis (Choma Bex 2021). The implementation of these methods, and more specifically the revision of the emission of fluid particles from the trailing edges of thick blades, currently present some difficulties. However, the preliminary results confirm that this complete model will allow for detailed results including a local distribution of loads on accurately rendered turbine geometries, together with the ensuing wakes.

2.2.3 *Simulation of the turbine by lifting line*

In the meantime, in order to have access within the Dorothy code to reliable and more immediate results in terms of loads, a lifting line alternative, named here LL-VPM, has been added to represent the turbines. Lifting line details can be found in (Katz & Plotkin 2001, van Garrel 2003, Shaler et al. 2020).

The turbine blades are represented by a given number of linear elements, for which a relative velocity $v_{rel} = \|\overrightarrow{\boldsymbol{v_{rel}}}\|$ and an angle of attack α are estimated at each time step, as shown by Figure 3. $\overrightarrow{\boldsymbol{v_{rel}}}$ takes into account the upstream velocity $\boldsymbol{U}^{\infty}$, the local tangential velocity induced by rotation and the induction velocity due to the wake $\boldsymbol{U}^{\psi}$. The lift $L\overrightarrow{\boldsymbol{e_L}}$ and drag $D\overrightarrow{\boldsymbol{e_D}}$ on each section are then computed using tabulated values of the lift and drag coefficients C_L and C_D, that are a function of the blade profile, α and Re.

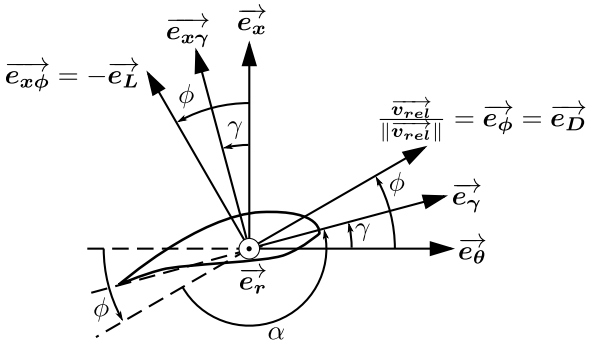

Figure 3: Scheme of the cross-section of a turbine blade section.

The bound circulation Γ_B for each blade section can be estimated with the Kutta-Jouvkowski theorem:

$$\Gamma_B(r,t) = \frac{1}{2} c v_{rel} C_L \ , \tag{17}$$

with r the radial distance and c the local chord.

According to (Murray & Barone 2011), the circulations Γ_T and Γ_S, shed respectively in the trailing and spanwise directions, can be deduced from the bound circulation distribution:

$$\Gamma_T\left(r - \frac{\mathrm{d}r}{2}, t\right) = \Gamma_B(r,t) - \Gamma_B(r - \mathrm{d}r, t) \ , \tag{18}$$

$$\Gamma_S(r,t) = \Gamma_B(r, t - \mathrm{d}t) - \Gamma_B(r,t) \ , \tag{19}$$

with $\mathrm{d}t$ the time step and $\mathrm{d}r$ the distance between blade sections.

In order to highlight the enhancement of performance prediction thanks to the LL-VPM, a cross comparison on the NREL 5-MW offshore wind turbine is conducted. While the geometry of the turbine and C_L, C_D data for the different blade profiles come from (Jonkman et al. 2009), the operating point at $TSR = 7$ is from (Dose et al. 2018) where detailed CFD results of the aerodynamic loads on the NREL 5-MW are available.

For the in-house LL-VPM and BEM, blades are discretized in 20 sections. Glauert's tip losses are used in the BEM code. LL-VPM computation uses a time step of $\mathrm{d}t = 0.03$ s, equivalent of 2 degrees of rotation, with an overall physical time of 25 s to reach the steady state. The computation runs on 140 cores during 1 hour, 20 minutes. Global performance with power and thrust coefficient, defined in Equation 20, is presented in Table 1.

$$C_P = \frac{P}{\frac{1}{2}\rho\pi R^2 \|\boldsymbol{U}^{\infty}\|^3} \qquad C_T = \frac{T}{\frac{1}{2}\rho\pi R^2 \|\boldsymbol{U}^{\infty}\|^2}, \tag{20}$$

where ρ is the fluid density, R is the hub radius plus blade length, P and T are respectively the aerodynamic power and thrust of the turbine at the steady state.

Table 1: NREL 5-MW (Jonkman et al. 2009) offshore wind turbine performance.

Method	C_P	C_T
CFD (Dose et al. 2018)	0.49	0.77
LL-VPM	**0.51**	**0.77**
BEM	0.48	0.75

LL-VPM results are very closed to the BEM and CFD that are reference methods. However the power coefficient seems slightly overestimated. C_P and C_T are integrated results. As a matter of thorough comparison, radial distribution of normal and tangential force densities are also studied in Figures 4 and 5.

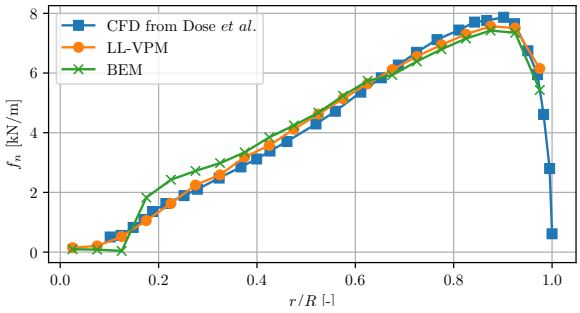

Figure 4: NREL 5-MW offshore wind turbine radial distribution of normal force density f_n.

Radial distribution of normal force density f_n shows a very good agreement for the 3 methods,

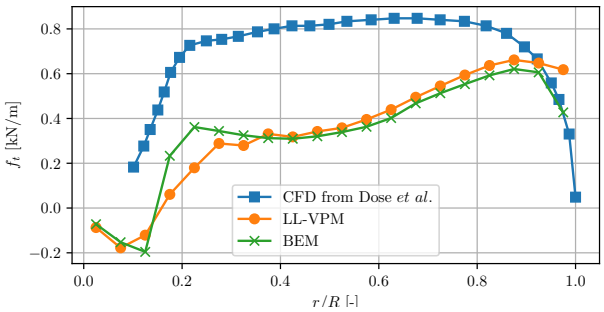

Figure 5: NREL 5-MW offshore wind turbine radial distribution of tangential force density f_t.

which tends to validate LL-VPM. However, radial distribution of tangential force density f_t shows some discrepancies. Differences of the same order of magnitude on the NREL 5-MW for equivalent methods are presented in (Schweigler 2012). BEM and LL-VPM seem to underestimate f_t mainly close to the blade root. In this region, the angles of attack can be high, thus, blade sections can be close to stall domain. Some phenomenon that can occur in this domain are not well described by C_L, C_D polar curves whereas CFD method represents them with greater accuracy. This must be part of the explanation of the discrepancies on f_t distribution.

2.3 *Simulation of the ambient turbulence*

Two alternatives for the representation of ambient turbulence are now integrated to the simulation code: the *Syntehtic Eddy Method* (SEM) initially described in (Jarrin et al. 2006), as well as a physically advantageous alternative based on the adaptation of the SEM formulated in (Poletto 2014).

The integration of fluctuations in the incoming velocity is justified by a Reynolds decomposition of the term representing the incoming velocity $\boldsymbol{U}^\infty = \mathbf{u}_\infty(\mathbf{x}, t)$:

$$\mathbf{u}_\infty(\mathbf{x}, t) = \overline{\mathbf{u}_\infty}(\mathbf{x}) + \mathbf{u}'(\mathbf{x}, t), \tag{21}$$

where $\bar{\cdot}$ designates the mean value of the function $\cdot$ and $\cdot'$ its fluctuating component, assumed to have an average of zero.

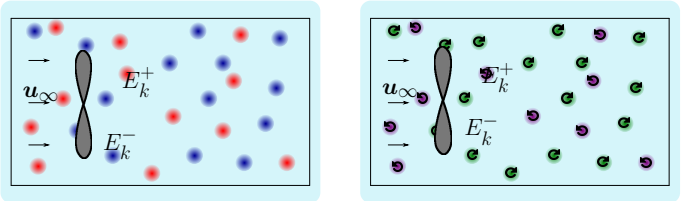

Figure 6: Schematic representation of the study area of volume V_0 disrupted by turbulent structures in the form of velocity sources and sinks for the SEM (left), or "eddies" for the DFSEM (right).

Jarrin *et al.* consider the fluctuating velocity u' as a perturbation induced by N *turbulent structures* (see Figure 6) randomly placed in a given study box of volume V_0:

$$\mathbf{u}'(\boldsymbol{x}) = \frac{1}{\sqrt{N}} \sum_{k=1}^{N} \mathbf{c}^\mathbf{k} f_\lambda \left(\frac{\mathbf{x} - \mathbf{x}^k}{\lambda} \right). \tag{22}$$

c_k is an intensity attributed to each turbulent structure, calibrated so as to ensure the statistical reproduction of any chosen Reynolds Stress Tensor $\overline{\overline{R}}$. f_λ is a shape function based on a gaussian shape, ensuring that the influence of each turbulent structure is limited to its radius $\boldsymbol{\lambda}$ in each dimension. A random sign $\boldsymbol{\epsilon}_k = +1$ or -1 makes of each turbulent structure either a velocity source or a velocity sink (independently in each dimension).

The details of this implementation within the framework of the Vortex Particle Method are presented in (Choma Bex et al. 2020). The quality of the reproduction of the Reynolds Stress Tensor given as a parameter is studied depending on various parameters of the method (number and size of turbulent structures for instance). A linear relation is evidenced between the turbulent structure sizes $\boldsymbol{\lambda}$ prescribed to this statistical method and the integral length scale of the turbulent behavior of the resulting flows (see Figure 8). With the addition of a parameter introducing variations on the sizes of the turbulent structures around their given mean values $\boldsymbol{\lambda}$, the power spectral densities thus produced approach the results expected both theoretically and by comparison with experimental data (see Figure 7).

Finally, the interaction between this model and tidal turbine simulations confirms the qualitative influence of the turbulent intensity produced by this model, which tends to progressively shorten the wakes as evidence by the wake lines of Figure 9. Figure 10 shows comparisons with experimental results satisfyingly validating the wakes obtained at high turbulence intensities.

Despite these promising results, one major drawback of the SEM resides in the fact that the disruption u' generated by the velocity sources and sinks is not divergence free, and thus the resulting flows no longer verify the incompressibility condition. An alternative formulation for the velocity disruption is necessary to ensure the physical consistency of this model, and to this end we have chosen the Divergence Free SEM (DFSEM) method formulated by (Poletto 2014).

This method is based on the same principle of turbulent structures evolving through a given study space, however the velocity disruption generated by each turbulent structure is now closer to the form of the Biot and Savart kernel at the heart of the Vortex Particle Method:

$$\mathbf{u}'(\mathbf{x}) = \frac{1}{\sqrt{N}} \sum_{k=1}^{N} \mathbf{K}_\lambda \left(\frac{\mathbf{x} - \mathbf{x}^\mathbf{k}}{\lambda} \right) \times R(\mathbf{d}^\mathbf{k}). \tag{23}$$

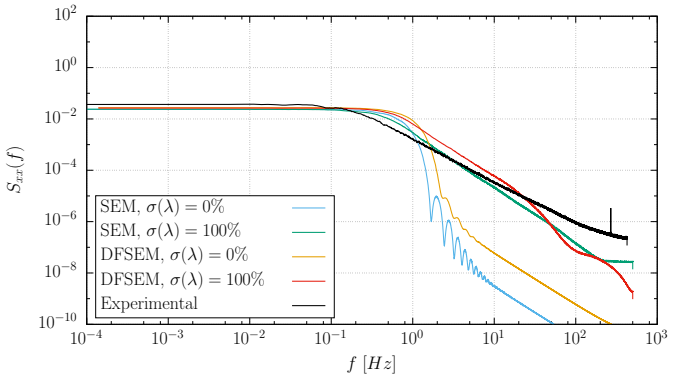

Figure 7: Power Spectral Densities (PSD) in a disrupted flow in the absence of turbines, with or without a variation $\sigma(\lambda)$ on the turbulent structure sizes λ , for both the SEM and DFSEM version of the velocity disruption formulation.

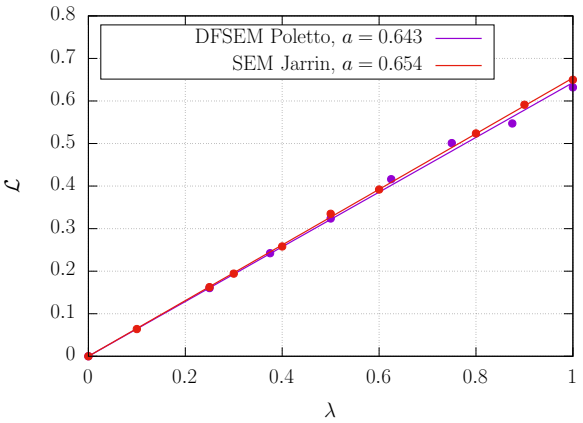

Figure 8: Integral length scale $\mathcal{L}$ of the turbulent behavior in disrupted flows in the absence of turbines, depending on the mean size λ of the turbulent structures given as a parameter to both the SEM and DFSEM versions of the velocity disruption calculations.

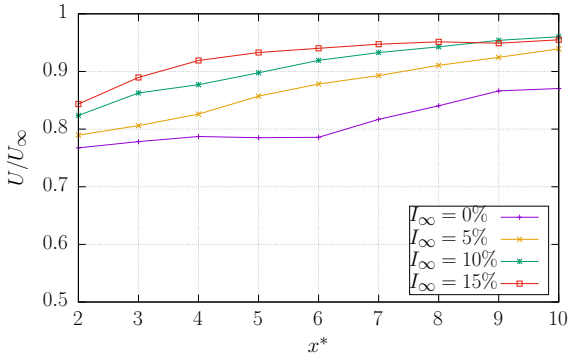

Figure 9: Velocity integrated on discs at set distances in the wake of a turbine (placed à $x^* = 0$), with varying turbulent intensities generated with the SEM method.

N is once more the number of turbulent structures k, however unlike the previous formulation the vector $\mathbf{K}_\lambda$ is derived from the Biot and Savart kernel as $\mathbf{K}_\lambda(\mathbf{y}) = \frac{g_\lambda(|\mathbf{y}|)}{|\mathbf{y}|^3}$, with g_λ a suitable shape function. Randomly chosen signs $\boldsymbol{\epsilon}_k = +1$ or -1 dictate here the direction of the "eddy" thus obtained. Intensities $\boldsymbol{c}_k$ are once more assigned to each turbulent structure, however this version of their formulation implies stronger restrictions on the Reynolds Stress Tensors which can be reproduced. While the present implementation is detailed in (Choma Bex et al. 2020), more information on the derivation and justification

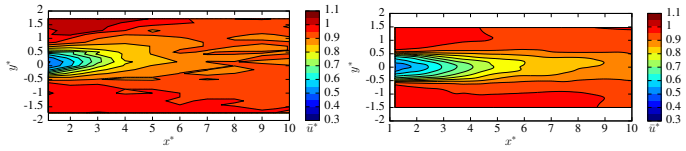

(a) Experimental (IFREMER)

(b) Numerical (SEM)

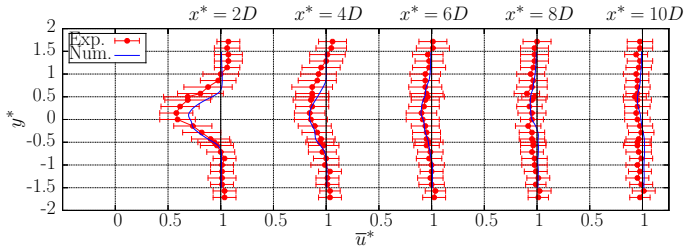

(c) Velocity profiles

Figure 10: Comparison between the wake of a single turbine at high turbulent intensity ($I_\infty = 15\%$), obtained experimentally at the flume tank of IFREMER in Boulogne sur Mer and numerically using the SEM method.

of these formulations are available in (Poletto 2014) Despite the different formulations for the velocity disruption $\boldsymbol{u}'$ Figures 7 and 8 confirm a similar behavior to that observed with the SEM in terms of PSD and correspondence between turbulent structure sizes and integral scale.

3 TURBINE WAKE INTERACTIONS IN REALISTIC OPERATING CONDITIONS

As an example of possible applications of the methods presented previously, this Section will treat of interactions within the four-turbine tidal array considered in the framework of the project NEPTHYD. Figure 11 presents this configuration in the surrounding environment of the Alderney Race.

This project, abandoned by its initial conceptors due to issues with the acquisition of the turbines, has become relevant once more with a new developper's stated intention to install SIMEC-Atlantis turbines replacing the Alstom model. A notable aspect of this configuration and its implantation site is the possibility for the wake of the central upstream turbine to strongly affect the downstream turbine within certain conditions of angular asymmetry in the incoming tidal current (which can vary by 15° to 20°). The lower part of Figure 11 shows the configurations considered for simulations which will be presented in the following paragraphs.

First of all, paragraph 3.1 will present the wake interactions obtained with various parameters used in the generation of ambient turbulence, and the results obtained in this realistic configuration. The results presented here are entirely sourced from (Slama et al. 2021), where more details are provided on the

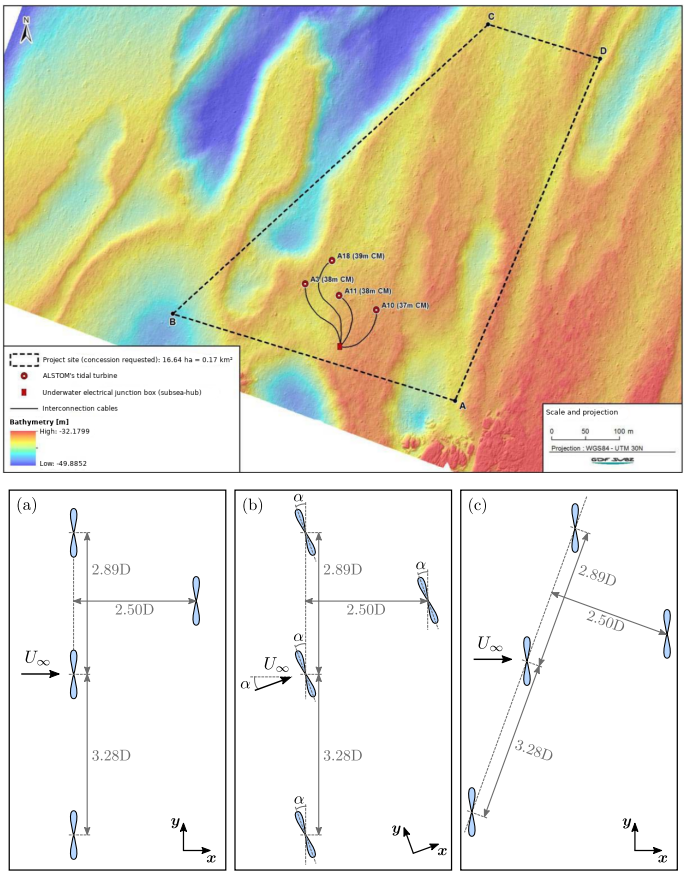

Figure 11: Configuration of the NEPTHYD project: a pre-commercial four turbine aray developped by Engie in 2014, which would have been outfitted with Alstom's Oceade™ turbines. This image, sourced from the report of the french Autorité Environnementale (Environnementale 16th), is reproduced from (Slama et al. 2021). The three following graphs show the array configuration taken from this report, and how it can be tilted for some simulations in order to reproduce the effect of the angle of the incoming upstream velocity and resulting yaw.

methods used and finer analyses of are carried out on wakes produced under varying conditions. Finally, making use of the recently added lifting line model, the last paragraph 3.2 will treat the fluctuations in loads perceived by the downstream turbine when tidal asymmetry in the incoming flow varies from 5° to 20°.

3.1 *Simulation of wake interactions in realistic conditions*

The motivation for this work carried out by Myriam Slama was to evaluate the degree of wake interaction between turbines in varying flow conditions. Among other metrics, this included the evaluation of velocity fluctuations right in front of the downstream turbine in order to have an initial estimation of the fluctuation of loads perceived by this machine. To this end, the thin-profile integral boundary method was first used, including the turbine interaction routines and preconditioned BiCG-STAB acceleration of (Mycek et al. 2017).

Figure 12(a) shows the wakes obtained for the four turbines, with no tidal asymmetry, and no ambient turbulence in the surrounding flow. While this con-

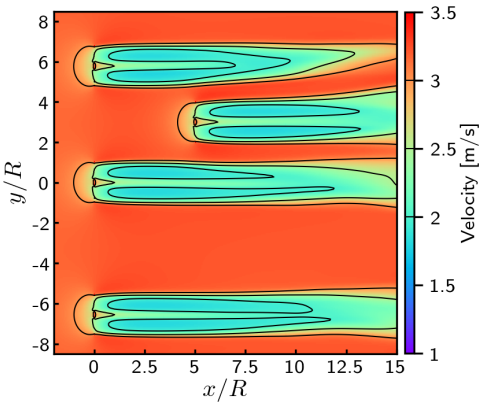

(a) $I_\infty = 0\%$

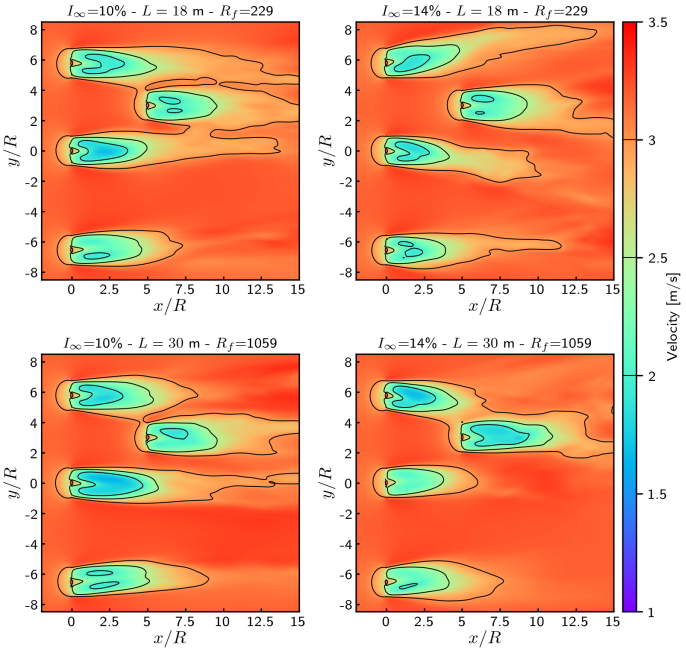

(b) varying I_∞ and $\mathcal{L}$

Figure 12: Time-averaged maps of the wakes of four interacting tidal turbines, without (upper part, $I_\infty = 0\%$) or with varying ambient turbulence conditions (lower part, varying I_∞ and integral length scales $\mathcal{L}$).

figuration is purely academic, it shows the ability of this software to simulate wakes extended to long distances, the Vortex Particle Method being rather conservative and well adapted to this type of simulation.

However in order to take into account way more realistic conditions of the surrounding flow, it is important to be able to consider an ambient turbulence intensity, along with its anisotropic ratio and characteristic length scale. In the context of projects such as the ANR THYMOTE or HYD2M, ambient turbulence levels and characteristics have been measured in the Alderney Race. The results obtained in (Sentchev et al. 2020) are chosen as reference values, owing to the proximity of their localization to the site considered here as well as a depth close to that of the prospective turbine centers.

The velocity maps of Figure 12(b) show the wakes

obtained for this configuration with $II = 10\%$ or 14% and $\mathcal{L} = 18\,m$ or $30\,m$, R_f being a purely numerical parameter with little effect on these results. Few variations are observed depending on these parameters, although a more detailed analysis is presented in (Slama et al. 2021). However major differences are evidenced compared to the laminar case, confirming the importance of the addition of the ambient turbulence generation model. A study of the variation in angles of tidal asymmetry in the incoming flow, and the resulting fluctuations perceived by the downstream turbine, is carried on in (Slama et al. 2021). It can generally be concluded that the lower the ambient turbulence levels, the more prominent the wakes will be and the more interaction will occur. Such configurations will be presented in the following paragraph, where a different method is used to evaluate the resulting fluctuations in loads on the downstream turbine.

3.2 *Estimation of the fluctuation of loads on a downstream turbine*

Older studies carried out in the Alderney Race have provided various assessments of tidal angular asymmetry, including on sites very close to that of our case study. These results confirm that the flow is not purely two-directional, but rather asymmetric in terms of both maximal velocity and incoming velocity angle. Near this location, an angular asymmetry of approximately 20° has been evidenced. In order to treat these cases of angular asymmetry which will result in strong interactions between the wakes of the upstream and downstream turbines (see configuration (c) of Figure 11), the use of the lifting line representation of the turbines will allow us to obtain our first results in terms of fluctuations in performances.

The wake maps of Figure 13 clearly show that the wake interactions between the central upstream turbine and the downstream turbine are stronger the higher the value of asymmetry angle. In this graph reproduced from (Slama et al. 2021), the points labelled 1 to 6 represent velocity probes of which the output is further analysed in this article. Thus, comparisons can be carried out confirming the coherence in terms of wakes between the representations of the turbines by the boundary integral method or the lifting line model.

The advantage of this new approach resides in the possibility to evaluate the levels of fluctuations in loads on the downstream turbine depending on various parameters. Figure 14 shows the average power coefficients $\overline{C_P}$ normalized into values noted $\overline{C_P^*}$, as well as the fluctuations in loads represented by the standard deviations $\sigma\left(C_P^*\right)$, for the configurations of the previous Figure 13. From these results, the following conclusions can be drawn:

- The upstream turbine represented in blue on the power curves functions as expected in a classic isolated case, with values of $\overline{C_P^*}$ close to 1 and few variations on the fluctuations of loads.

- No significant difference in $\overline{C_P^*}$ between the two turbines is apparent for $\alpha = 5$, 10 or 15°. A slightly higher value of $\overline{C_P^*}$ for the downstream turbine at $\alpha = 5$ could be attributed to a Venturi effect causing an acceleration between two upstream turbines (see Figure 13), which seems to disappear for higher angles of incidence. However, a strong loss of $\overline{C_P^*}$ is evidenced for $\alpha = 20°$, due to the direct interaction of the downstream turbine with the upstream wake.

- The fluctuation of loads for the downstream turbine increases with the angle of incidence, possibly due do an average velocity gradient as well as the turbulence generated by the upstream turbines' wake. This increase can be estimated at $+50\%$ between 5° and 20°.

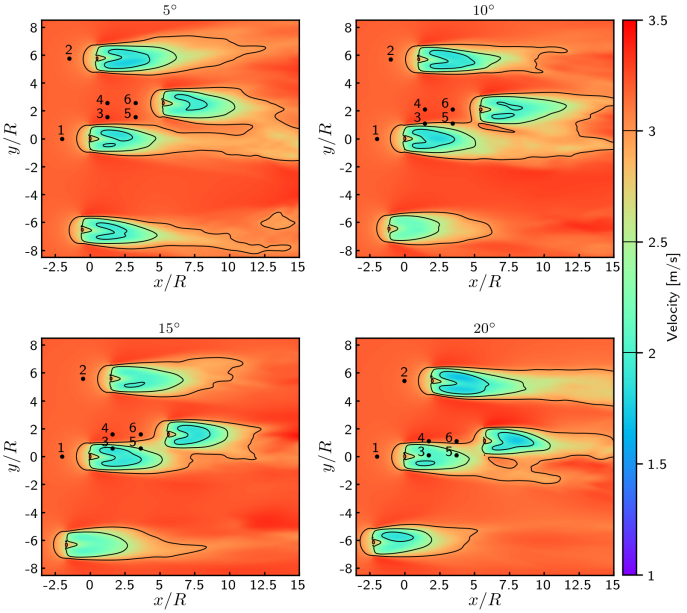

Figure 13: Time-averaged velocity maps of the wakes of four interacting turbines, with $I_\infty = 10\%$, $\mathcal{L} = 18m$, and various angles of inclination of the incoming velocity. These results are sourced from the conference paper (Slama et al. 2021) presented by Y. Ben Belkacem at EWTEC 2021.

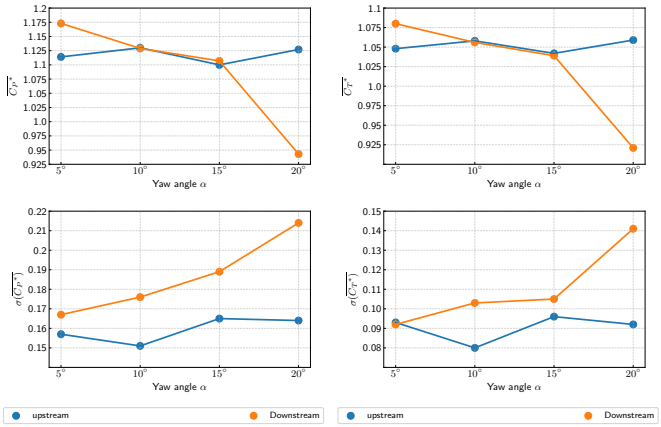

Figure 14: Average values and standard deviations of performance measures reproduced from (Slama et al. 2021).

As mentioned in (Slama et al. 2021), these results are preliminary and should be treated with some reserve. However, the potential of the combination of methods present in the simulation code is believed to have become clear.

4 CONCLUSION

The Lagrangian Vortex code Dorothy includes to this day two working alternatives for the representation of tidal or wind turbines, namely a boundary integral method applied to a simplified geometry of the turbine blades or a lifting line using tabulated values. While the first option gives access to a detailed resolution of the wake, the second allows for more immediate and assured results in terms of performance at a lower computational cost. A third alternative is under development in order to extend the boundary integral method to fully rendered thick blade profiles on which can be obtained a local distribution of loads.

Two alternatives are now present in order to emulate the disruptive effect of ambient turbulence in a given study area covering the entirety of the considered wakes. A first implementation based on Jarrin's SEM has been thoroughly studied and validated. In the absence of turbines, these validations included the verification of the reproduction of any requested Reynolds Stress Tensor, the quality of the PSD under appropriately adapted conditions and the straightforward calibration of the integral length scale of produced turbulent behavior depending on a given size parameter. The turbulent flows thus generated were also validated in their interaction with turbine wakes, by comparison with experimental results and by their qualitative influence on the shortening of the wakes. A more physically consistent alternative has been added in the form of Poletto's DFSEM, sharing a remarkable number of characteristics with the SEM in the absence of turbines. The investigation of the interaction of this method for the computation of velocity disruptions with tidal or wind turbine wakes remains to be completed. Developments are also underway on the distribution of turbulent structure sizes so that these statistical models may better represent the underlying physics of a turbulent flow, while also promising improvements on some issues of over-dissipation of wakes at low turbulent intensities.

The application of the current singularity method and the lifting line model combined with the SEM and various algorithmic considerations has allowed for the simulation of a real pre-commercial tidal farm configuration in the true conditions of its local projected implantation site. Relevant conclusions were reached on the impact of ambient turbulence and tidal asymmetry causing variations in the angle of the incoming flow in this particular area. For instance, the development of an area of induction of an upstream turbine on the downstream turbine can be observed, the undesirable repercussions of which are then evidenced by a drop in average performance results together with an increase in their fluctuations.

Further developments of this simulation code are under consideration in order to take into account as many as possible of the realistic operating conditions present in tidal or wind turbine implantation sites. Among these additions figure the possibility to allow for gradients or various profiles in the incoming velocity, the addition of a Stokes type wave generation model for tidal simulations, and further on once a detailed distribution of loads can be obtained on the turbine bodies the possibility to treat the impact of all such velocity fluctuations with a structural model for fatigue and deformations of the turbine blades. The final goal of this work is to develop a complete simulation tool, able to consider all means of realistic operating conditions, with alternative methods depending on the type of results as well as precision and computational times desired.

ACKNOWLEDGEMENTS

The authors would like to acknowledge the support of the Interreg TIGER project funding the continuation of this work, along with IFREMER for its funding and co-funding of multiple PhD works on this subject. This work was carried out using computational resources of the CRIANN (Centre Régional Informatique et d'Applications Numériques de Normandie).

REFERENCES

Bousquet, J. (1990). *Méthode des singularités*. Cépaduès - Editions.

Choma Bex, C. (2021). *Développement de modèles numériques Lagrangiens pour la simulation du comportement d'hydroliennes*. Ph. D. thesis, Université Le Havre Normandie.

Choma Bex, C., C. Carlier, A. Fur, G. Pinon, G. Germain, & E. Rivoalen (2020). A stochastic method to account for the ambient turbulence in lagrangian vortex computations. *Applied Mathematical Modelling 88*, 38 – 54.

Choma Bex, C., G. Pinon, M. Slama, B. Gaston, G. Germain, & E. Rivoalen (2020, 28 sept - 02 October). Lagrangian Vortex computations of turbine wakes: recent improvements using Poletto's Synthetic Eddy Method (SEM) to account for ambient turbulence. In *The Science of Making Torque from Wind (TORQUE 2020)*, Delft, The Netherlands.

Cottet, G. & P. Koumoutsakos (2000). *Vortex methods: theory and practice*. Cambridge University Press.

Dose, B., H. Rahimi, I. Herráez, B. Stoevesandt, & J. Peinke (2018). Fluid-structure coupled computations of the nrel 5 mw wind turbine by means of cfd. *Renewable Energy 129*, 591–605.

Environnementale, A. A. (last acces 2016, June the 16th). Projet nepthyd. Technical report, Conseil Général de l'environement et du développement durable: http://www.cgedd.developpement-durable.gouv.fr.

Greco, L., F. Salvatore, & F. D. Felice (2004, August). Validation of a quasi–potential flow model for the analysis of marine propellers wake. In *Twenty-Fifth Symposium on Naval Hydrodynamics*, St. John's, Newfoundland, Canada.

Jarrin, N., S. Benhamadouche, D. Laurence, & R. Prosser (2006). A synthetic-eddy-method for generating inflow conditions for large-eddy simulations. *International Journal of Heat and Fluid Flow 27*, 585–593.

Jonkman, J., S. Butterfield, W. Musial, & G. Scott (2009). Definition of a 5-mw reference wind turbine for offshore system development. Technical Report NREL/TP-500-38060, National Renewable Energy Lab. (NREL), Golden, CO (United States).

Katz, J. & A. Plotkin (2001). *Low-Speed Aerodynamics*. Cambridge University Press.

Lewis, R. (1991). *Vortex element methods for fluid dynamic analysis of engineering systems*. Cambridge University Press.

Lindsay, K. & R. Krasny (2001). A particle method and adaptive treecode for vortex sheet motion in three-dimensional flow. *Journal of Computational Physics 172*(2), 879–907.

Morino, L. (1990). *Nonlinear Problems of Fluid Dynamics*, Volume 6 of *Developments in Boundary Element Methods*, Chapter Helmholtz and Poincaré Potential-Vorticity Decompositions for the Analysis of Unsteady Compressible Viscous Flows, pp. 1–54. Elsevier Applied Science Publishers.

Murray, J. & M. Barone (2011). *The Development of CACTUS, a Wind and Marine Turbine Performance Simulation Code*.

Mycek, P. (2013). *Étude numérique et expérimentale du comportement d'hydroliennes*. Ph. D. thesis, Université du Havre.

Mycek, P., G. Pinon, G. Germain, & E. Rivoalen (2016). Formulation and analysis of a diffusion-velocity particle model for transport-dispersion equations. *Computational and Applied Mathematics 35*(2), 447–473.

Mycek, P., G. Pinon, C. Lothodé, A. Dezotti, & C. Carlier (2017). Iterative solver approach for turbine interactions: application to wind or marine current turbine farms. *Applied Mathematical Modelling 41*, 331 – 349.

Ogami, Y. (2017). A three-dimensional source-vorticity method for simulating incompressible potential flows around a deforming body without the kutta condition. *Computers and Fluids 154*, 184–199.

Pinon, G., C. Carlier, A. Fur, B. Gaurier, G. Germain, & E. Rivoalen (2017). Account of ambient turbulence for turbine wakes using a synthetic-eddy-method. *Journal of Physics: Conference Series 854*(1), 012016.

Pinon, G., P. Mycek, G. Germain, & E. Rivoalen (2012). Numerical simulation of the wake of marine current turbines with a particle method. *Renewable Energy 46*(0), 111 – 126.

Poletto, R. (2014). *Divergence free develoment of the Synthetic Eddy Method in order to improve synthetic turbulence for embedded LES simulations*. Ph. D. thesis, University of Manchester.

Rehbach, C. (1977). Calcul numérique d'écoulements tridimensionnels instationnaires avec nappes tourbillonaires. *La Recherche Aérospatiale 5*, 289–298.

Riziotis, V. A. & S. G. Voutsinas (2008). Dynamic stall modelling on airfoils based on strong viscous–inviscid interaction coupling. *International Journal for Numerical Methods in Fluids 56*(2), 185–208.

Salvatore, F., F. Bellotto, D. Calcagni, F. D. Felice, D. Dhomé, & J.-C. Allo (2015, 6-11th Sept. 2015). Validation of a computational hydrodynamics model for horizontal-axis marine current turbines. In *10th European Wave and Tidal Energy Conference (EWTEC)*. Nantes, France.

Salvatore, F., Z. Sarichloo, & D. Calcagni (2018, May). Marine turbine hydrodynamics by a boundary element method with viscous flow correction. *Journal of Marine Science and Engineering*.

Salvatore, F., C. Testa, & L. Grego (2003, November). A viscous/inviscid coupled formulation for unsteady sheet cavitation modelling of marine propellers. In *Fifth International Symposium on Cavitation*, Osaka, Japan.

Schweigler, K. M. (2012). Aerodynamic analysis of the nrel 5-mw wind turbine using vortex panel method. Master's thesis, Department of Applied Mechanics, Division of Fluid Dynamics, Chalmers University of Technology.

Sentchev, A., M. Thiébaut, & S. Guillou (2020). *Turbulence characterization at tidal-stream energy site in Alderney Race* (CRC Press ed.).

Shaler, K., E. Branlard, & A. Platt (2020). Olaf user's guide and theory manual. Technical Report NREL/TP-5000-75959, Golden, CO: National Renewable Energy Laboratory.

Slama, M., C. Choma Bex, G. Pinon, M. Togneri, & I. Evans (2021). Lagrangian vortex computations of a four tidal turbine array: an example based on the NEPTHYD layout in the alderney race. *Energies 14*(13).

Slama, M., G. Pinon, Y. Ben Belkacem, C. Choma Bex, M. Togneri, & I. Evans (2021, Sep 5–9). Fluctuating loads perceived by the downstream turbine in a farm. In D. Greaves (Ed.), *Proceedings of the Fourteenth European Wave and Tidal Energy Conference*, University of Plymouth, UK, pp. 1–8. EWTEC. ISSN: 2309-1983.

van Garrel, A. (2003). Development of a wind turbine aerodynamics simulation module. Technical Report ECN-C–03-079, Energy research Centre of the Netherlands.